

Dense Prediction with Attentive Feature Aggregation

Yung-Hsu Yang¹, Thomas E. Huang², Samuel Rota Bulò³, Peter Kotschieder³, Fisher Yu²

¹ National Tsing Hua University, Taiwan

² ETH Zürich

³ Facebook Reality Labs

royyang@gapp.nthu.edu.tw, thomas.huang@vision.ee.ethz.ch, rotabulo@fb.com, pkotschieder@fb.com, i@yf.io

Abstract

Aggregating information from features across different layers is an essential operation for dense prediction models. Despite its limited expressiveness, feature concatenation dominates the choice of aggregation operations. In this paper, we introduce Attentive Feature Aggregation (AFA) to fuse different network layers with more expressive non-linear operations. AFA exploits both spatial and channel attention to compute weighted average of the layer activations. Inspired by neural volume rendering, we extend AFA with Scale-Space Rendering (SSR) to perform late fusion of multi-scale predictions. AFA is applicable to a wide range of existing network designs. Our experiments show consistent and significant improvements on challenging semantic segmentation benchmarks, including Cityscapes, BDD100K, and Mapillary Vistas, at negligible computational and parameter overhead. In particular, AFA improves the performance of the Deep Layer Aggregation (DLA) model by nearly 6% mIoU on Cityscapes. Our experimental analyses show that AFA learns to progressively refine segmentation maps and to improve boundary details, leading to new state-of-the-art results on boundary detection benchmarks on BSDS500 and NYUDv2. Code and video resources are available at <http://vis.xyz/pub/dla-afa>.

1 Introduction

Dense prediction tasks such as semantic segmentation and boundary detection are fundamental enablers for many computer vision applications. Semantic segmentation requires predictors to absorb intra-class variability while establishing inter-class decision boundaries. Boundary detection also requires an understanding of both fine-grained scene details and object-level boundaries. Many computer vision tasks share those requirements and a common solution is to use multi-scale representations to strike a balance between preserving details and maintaining relevant context.

There are two major approaches to obtaining effective multi-scale representations. Dilated convolutions [41] can aggregate context information while preserving spatial information. Most of the top performing segmentation methods adopt this approach [6, 48, 42, 32] to extract contextual pixel-wise information. The drawback of this approach is the extensive usage of layer memory for storing high-resolution feature maps. An alternative approach is to progressively down-sample the layer resolution as *e.g.* in image classification networks and then upsample the resolution by aggregating

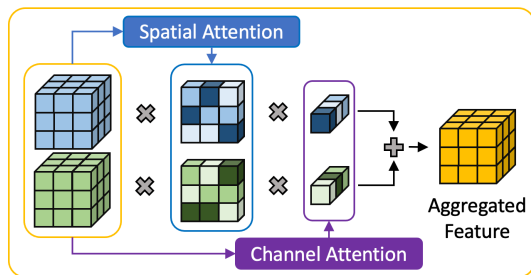


Figure 1: Attentive Feature Aggregation. We use attention to aggregate different scale or level information and gain a rich representation for dense prediction.

information from different layer scales with layer concatenations [20, 43, 27]. Methods using this approach achieve state-of-the-art results with reduced computational efforts and fewer parameters [33]. Even though many works design new network architectures to effectively aggregate multi-scale information, the predominant aggregation operations are still feature concatenation or summation [27, 20, 33, 43, 47]. These linear operations do not consider feature interactions or selections between different levels or scales.

We propose *Attentive Feature Aggregation (AFA)* as a non-linear feature fusion operation to replace the prevailing tensor concatenation or summation strategies. Our attention module uses both spatial and channel attention to learn and predict the importance of each input signal during fusion. Aggregation is accomplished by computing a linear combination of the input features at each spatial location, weighted by their relevance. Compared to linear fusion operations, our AFA module can take into consideration complex feature interactions and attend to different feature levels depending on their importance. AFA introduces negligible computation and parameter overhead and can be easily used to replace fusion operations in existing methods, such as skip connections. Figure 1 illustrates our attentive feature aggregation (AFA).

Inspired by neural volume rendering [11, 21], we propose *Scale-Space Rendering (SSR)* as a novel attention computation mechanism to fuse multi-scale predictions. We treat those predictions as sampled data in scale-space and design a coarse-to-fine attention concept to render final predictions.

We demonstrate the effectiveness of AFA when applied to

a wide range of existing networks on both semantic segmentation and boundary detection benchmarks. We plug our AFA module into various popular segmentation models: FCN [20], U-Net [27], HRNet [33], and Deep Layer Aggregation (DLA) [43]. Experiments on several challenging semantic segmentation datasets including Cityscapes [8], Mapillary Vistas [23], and BDD100K [40] show that AFA can significantly improve the segmentation performance of each representative model. Additionally, *AFA-DLA* has competitive results compared to the state-of-the-art models despite having fewer parameters and using less computation. We also observe that AFA learns to attend to different types of details depending on the input properties and performs progressive refinement. Furthermore, on the boundary detection datasets BSDS50 [1] and NYUDv2 [29], *AFA-DLA* achieves state-of-the-art performances. We conduct comprehensive ablation studies to validate the advantages of each component of our AFA module. Our source code will be released.

2 Related Work

Recent semantic segmentation and boundary detection methods are based on fully convolutional networks [20] and focus on incorporating different components to the architecture to improve the performance, such as multi-scale context, multi-scale inference, and deep aggregation.

Multi-Scale Context To better handle fine details, segmentation models use the convolutional trunk with low output stride. However, this causes a slow increase of the receptive field and thus limits the semantic information contained in the final feature. Some works utilize dilated backbones [41] to enlarge the receptive field to address this problem. PSP-Net [48] uses a Pyramid Pooling Module (PPM) to generate multi-scale context and fuse them as the final feature. The DeepLab models [6] use Atrous Spatial Pyramid Pooling (ASPP) to assemble context from multiple scales generated by several parallel atrous convolutions, yielding denser and wider features. BDCN [15] applies dilated convolutions through Scale Enhancement Modules (SEM) to enrich the multi-scale representation for boundary detection. Recently, many works [36, 18, 13] continue to explore the potential of multi-scale context. In contrast, our *AFA-DLA* architecture uses attention to conduct multi-scale feature fusion extensively to increase the receptive field without using expensive dilated convolutions. Thus, our model can achieve comparable performance with much less computation and fewer parameters.

Multi-Scale Inference Many computer vision tasks leverage multi-scale inference to get higher performance. The most common way to fuse the multi-scale results is using average pooling [3, 4, 43, 17, 7], but it applies the same weighting to each scale and thus may not be the optimal solution. Some approaches use an explicit attention model [5, 37] to learn a suitable weighting for each scale and get further improvement in performance. However, the main drawback of an explicit model is the increased computational requirement for evaluating multiple scales. To overcome this problem, [31] proposes a hierarchical attention mechanism that only needs two scales during training but can utilize more

scales during inference. With their multi-scale attention, they achieved state-of-the-art results on Cityscapes [8] and Mapillary Vistas [23]. In this work, we propose SSR, a more robust multi-scale attention mechanism which generalises the hierarchical approach in [31], and exploits feature relationships in scale-space to further improve the performance.

Feature Aggregation Aggregation is widely used in the form of skip connections or feature fusion nodes in most deep learning models [20, 27, 33]. The Deep Layer Aggregation [43] network shows that higher connectivity inside the model can enable better performance with fewer parameters. Unlike linear aggregation, our AFA module leverages extracted spatial and channel information to efficiently select the essential features and to increase the receptive field at the same time. Moreover, it can be readily used to replace the standard tensor concatenation operation that is typically adopted in multi-scale architectures with attention mechanisms to merge the features [34, 47].

3 Method

In this section, we first introduce our attentive feature aggregation (AFA) module and extend our AFA to scale-space rendering (SSR) attention for multi-scale inference.

3.1 Attentive Feature Aggregation

Our attentive feature aggregation (AFA) module computes both spatial and channel attention based on the relation of the input feature maps. Those attention values are then used to modulate the input activation scales and produce one merged feature map. The operation is nonlinear in contrast to feature concatenation or summation. Unlike previous attention methods [2, 34, 12], AFA focuses on aggregating feature maps of different network layers to obtain more expressive representations. We use two different self-attention mechanisms to generate spatial and channel attentions for input feature $F \in \mathbb{R}^{C \times H \times W}$, as shown in Figure 2 (a) and (b).

The spatial attention uses a fully convolutional block ω_s to encode F . It is defined as

$$a_s \triangleq \sigma(\omega_s(F)),$$

where $a_s \in \mathbb{R}^{1 \times H \times W}$ and σ is the sigmoid activation.

For the channel attention, we first apply average pooling to get F^{avg} and max pooling to get F^{max} . Then, we use another fully convolutional block ω_c with a bottleneck input-output channel design to further transform features to F_c^{avg} and F_c^{max} . By summing them up with equal weighting and using sigmoid σ as the activation function, we can generate channel attention $a_c \in \mathbb{R}^{C \times 1 \times 1}$, i.e.,

$$a_c \triangleq \sigma(\omega_c(\text{AvgPool}(F)) + \omega_c(\text{MaxPool}(F))).$$

By combining both attention mechanisms, AFA enables the network to model complex feature interactions and attend to different features.

Binary Fusion We employ a simple attention-based aggregation mechanism using our spatial and channel attentions to replace standard binary fusion nodes. When merging two input feature maps, we apply channel and spatial attention

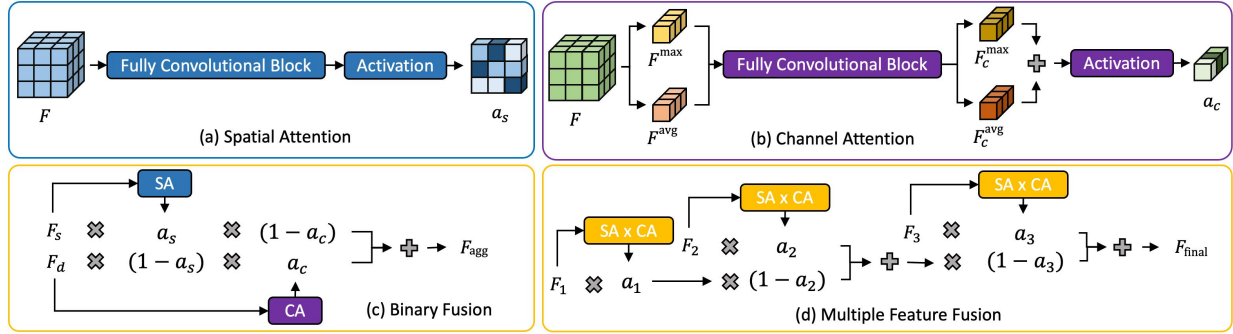


Figure 2: Attention Feature Aggregation. (a) Spatial Attention (SA) module. (b) Channel Attention (CA) module. (c) Binary fusion module for input features F_s and F_d . (d) Multiple feature fusion module for three input features F_1 , F_2 , and F_3 . $SA \times CA$ represents computing spatial and channel attention first and then using element-wise multiplication on a_c and a_s to get the final attention a_i for F_i .

sequentially. As shown in Figure 2 (c), when two features are aggregated, we denote one feature map as F_s and the other as F_d . Usually, F_s is the shallower feature representation. F_s is used to compute a_s , while F_d is responsible for a_c . This is because shallower layers will contain richer spatial information, and deeper layers will have more complex channel features. Then, we apply our proposed attention mechanism to aggregate the inputs and get the aggregated feature F_{agg} as

$$F_{agg} \triangleq a_s \odot (1 - a_c) \odot F_s + (1 - a_s) \odot a_c \odot F_d,$$

where \odot denotes element-wise multiplication (with broadcasted unit dimensions).

Multiple Feature Fusion We extend the binary fusion node to further fuse together multiple multi-scale features. Recent works [27, 33, 43] iteratively aggregate features across the model, but only exploit the final aggregated feature, neglecting intermediate features computed during the aggregation process. By applying our AFA module on these intermediate features, we give the model more flexibility to select the most relevant features.

Given k multi-scale features F_i for $i \in \{1, \dots, k\}$, we first order them based on the amount of aggregated information they contain, i.e., a feature with higher priority will have gone through a higher number of aggregations. Then, we compute both spatial and channel attention for each feature and take the product as the new attention. The combined attention a_i is defined as

$$a_i \triangleq SA(F_i) \odot CA(F_i),$$

where SA denotes our spatial attention function and CA our channel attention function. For fusing the multi-scale features, we perform hierarchical attentive fusion by progressively aggregating features starting from F_1 to F_k to obtain the final representation F_{final} as

$$F_{final} \triangleq \sum_{i=1}^k \left[a_i \odot F_i \odot \prod_{j=i+1}^k (1 - a_j) \right].$$

In Figure 2 (d), we show an example with $k = 3$. The new final representation F_{final} is an aggregation of features at multiple different scales, combining information from shallow to deep levels.

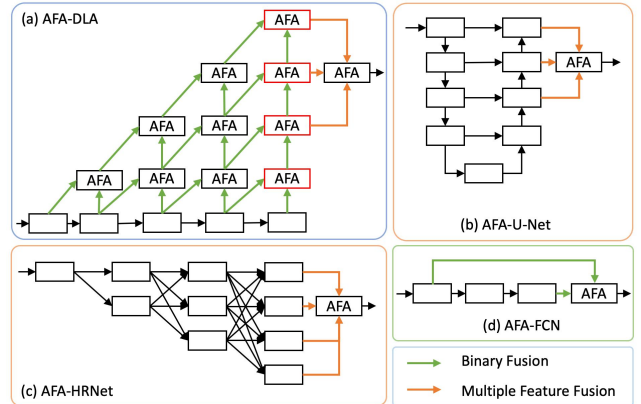


Figure 3: Segmentation models with our AFA module. We show parts of the original models related to feature aggregation and our modifications. Red blocks represent auxiliary segmentation head added during training.

We can apply our AFA module to widely used segmentation models, as shown in Figure 3. In U-Net [27] and HR-Net [33], we add our multiple feature fusion module to fully utilize the previously unused aggregated multi-scale features. In FCN [20], we simply replace the original linear aggregation node in the decoder with our attentive binary fusion. For DLA [43], we not only substitute the original aggregation nodes but also add our multiple feature fusion module. Due to the higher connectivity of its nodes, the DLA network can benefit more from our improved feature aggregation scheme, and thus we use AFA-DLA as our final model.

3.2 Scale-Space Rendering

Repeated use of attention layers may lead to numerical instability or vanishing gradients. We extend the above-mentioned attention mechanism to fuse the dense predictions from multi-scale inputs more effectively. The multi-scale predictions can be regarded as samples in a scale space representation. Our solution resembles a volume rendering scheme applied to the scale space. This scheme provides a hierarchical, coarse-to-fine strategy to combine features, leveraging a

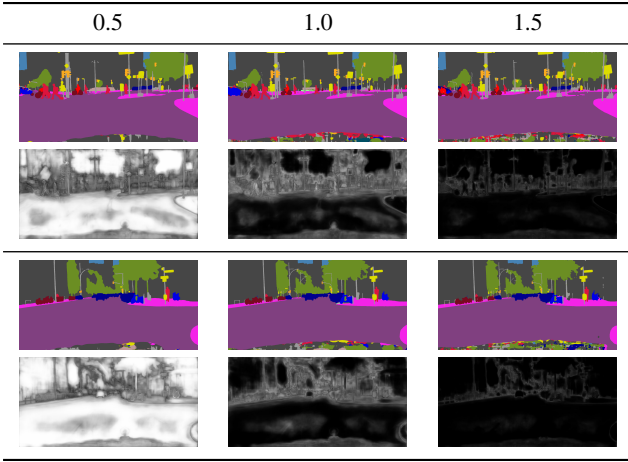


Figure 4: Visualization of attention maps generated by our scale-space rendering (SSR) attention. Whiter regions denote higher attention. SSR learns to focus on detailed regions in larger scale images and on lower frequency information in smaller scale images.

scale-specific attention mechanism. We will also show that our approach generalizes the hierarchical multi-scale attention method [31].

Without loss of generality, we focus on a single pixel and assume that our model provides a dense prediction for the target pixel at k different scales. The prediction for the i th scale is denoted by $P_i \in \mathbb{R}^d$. Accordingly, $P \triangleq (P_1, \dots, P_k)$ denotes the feature representation of the target pixel in our scale-space. Furthermore, we assume that $i < j$ implies that scale i is coarser than scale j .

Our target pixel can be imagined as a ray moving through scale-space, starting from scale 1 towards scale k . We redesign the original hierarchical attention in proposed multiple feature fusion mechanism and mimic the volume-rendering equation, where the volume is implicitly given by the scale-space. To this end, besides the feature representation P_i at scale i , we assume our model to predict for the target pixel also a scalar $y_i \in \mathbb{R}$ so that $e^{-\phi(y_i)}$ represents the probability that the particle will cross scale i , given some nonnegative scalar function $\phi: \mathbb{R} \rightarrow \mathbb{R}_+$. We can then express the scale attention α_i as the probability of the particle to reach scale i and stop there, i.e.

$$\alpha_i(y) \triangleq \left[1 - e^{-\phi(y_i)}\right] \prod_{j=1}^{i-1} e^{-\phi(y_j)},$$

where $y \triangleq (y_1, \dots, y_k)$.

Finally, the fused multi-scale prediction for the target pixel can be regarded as the ‘‘rendered’’ pixel, where the pixel features at the different scales P_i are averaged by the attention coefficients α_i following the volume rendering equations. Accordingly,

$$P_{\text{final}} \triangleq \sum_{i=1}^k P_i \alpha_i(y)$$

represents the feature for the target pixel that we obtain after fusing P across all scales with attention driven by y .

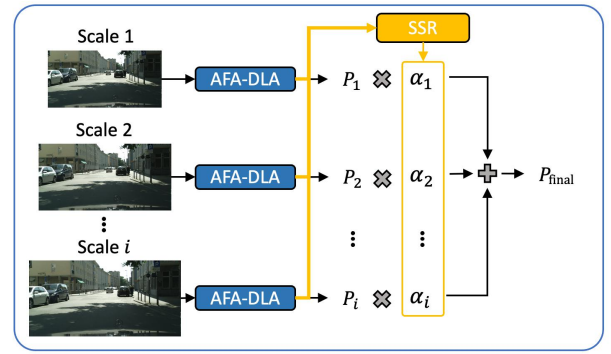


Figure 5: Overview of AFA-DLA with SSR. We use two scales [0.5, 1.0] during training and more scales during inference to pursue higher performance. SSR is our scale-space rendering attention module.

The proposed scale-space rendering (SSR) mechanism can be regarded as a generalization of the hierarchical multi-scale attention proposed in [31], for the latter can be obtained from our formulation by simply setting $\phi(y_i) \triangleq \log(1 + e^{y_i})$, i.e., ϕ is the soft-plus function, and by fixing $\phi(y_k) \triangleq \infty$.

Choice of ϕ In our experiments, we use the absolute value function as our ϕ , i.e. $\phi(y_i) \triangleq |y_i|$. This is motivated by a better preservation of the gradient flow through the attention mechanism, as we found existing attention mechanisms to suffer from vanishing gradient issues. For a detailed description of the aforementioned issue, refer to our appendix.

To understand which parts of the image SSR attends to at each scale, we visualize the generated attention maps in Figure 4. Detailed regions is handled better in larger scale images due to the higher resolution and the prediction for lower frequency region is often better in smaller scale images. Our SSR learns to focus on the right region for different scales and thus boost the final performance.

We combine our AFA-DLA model with SSR to produce the final predictions. As shown in Figure 5, AFA-DLA propagates information from different scales to the SSR module, which then generates attention masks α_i used to fuse the predictions P_i to get our final prediction P_{final} .

Training Details For fair comparison with other methods [44, 31], we reduce the number of filters from 256 to 128 in the OCR [44] module and add it after our AFA-DLA network to refine our final predictions. Our final model can be trained at k different scales. We use $k = 2$ for training and RMI [49] to be the primary loss function L_{primary} for our final prediction P_{final} . We add three different types of auxiliary cross-entropy losses to stabilize the training. First, we use the generated SSR attention to fuse the auxiliary per-scale predictions from OCR, yielding $P_{\text{ocr}}^{\text{aux}}$ and the loss L_{ocr} . Second, we compute and sum up cross-entropy losses for each scale prediction P_i yielding L_{scale} . Lastly, we add auxiliary segmentation heads inside AFA-DLA as in Figure 3 (a) and have predictions for each scale. We fuse them with SSR across scales and get P_j^{aux} , where $1 \leq j \leq 4$. We compute the auxiliary loss for each and sum then up as L_{dla}

Table 1: Segmentation results on Cityscapes validation set. We report the best performance from other approaches. AFA-DLA achieves state-of-the-art performance when compared to methods that do not use external datasets.

Method	mIoU
DLA-Up [43]	75.10
DeepLabV3+ [6]	79.55
Seg Fix [45]	83.22
DecoupleSegNets [17]	83.50
AFA-DLA-X-102 (Ours)	85.14

Table 2: Segmentation results on Cityscapes testing set. We only compare to published methods without using extra segmentation datasets. AFA-DLA also obtains competitive performance with the top performing method while using around 75% fewer operations and parameters.

Method	FLOPs (G)	Param.(M)	mIoU
DLA [43]	-	-	75.90
HRNet [33]	-	-	81.8
DeepLabV3+ [6]	2514	54.4	82.10
DecoupleSegNet [17]	6197	138.4	83.70
AFA-DLA-X-102 (Ours)	1333	36.3	83.58

Accordingly, the total loss function is the weighted sum as

$$L_{\text{all}} \triangleq L_{\text{primary}} + \beta_o L_{\text{ocr}} + \beta_s L_{\text{scale}} + \beta_d L_{\text{dla}},$$

where we set $\beta_o \triangleq 0.4$, $\beta_s \triangleq 0.05$ and $\beta_d \triangleq 0.05$. We illustrate more detail of each loss function in the appendix.

4 Experiments

We conduct experiments on several public datasets on both semantic segmentation and boundary detection tasks and conduct a thorough analysis with a series of ablation studies. Due to the space limit, we leave additional implementation details to our appendix.

4.1 Results on Cityscapes

The Cityscapes dataset [8] provides high resolution (2048 x 1024) urban street scene images and their corresponding segmentation maps. It contains 5K well annotated images for 19 classes and 20K coarsely labeled image as extra training data. Its finely annotated images are split into 2975, 500 and 1525 for training, validation and testing. We use DLA-X-102 as the backbone for our AFA-DLA model with a batch size of 8 and full crop size. Following [31], we train our model with auto-labeled coarse training data with 0.5 probability and otherwise use the fine labeled training set. During inference, we use multi-scale inference with [0.5, 1.0, 1.5, 1.75, 2.0] scales, image flipping, and Seg-Fix [46] post-processing. The results on the validation set are shown in Table 1 and on the test set in Table 2.

With only using ImageNet [9] pre-training and without using external segmentation datasets, AFA-DLA achieves 85.14 mean IoU on the Cityscapes validation set, achieving state-of-the-art performance. On the Cityscapes test set,

Table 3: Combining AFA with other widely used segmentation models on the Cityscapes validation set. Combined with our AFA module, each model can obtain at least 2.5% improvement in mIoU, with only a small computational and parameter overhead.

Method	FLOPs (G)	Param.(M)	mIoU	Δ (%)
FCN (R50)	1581.8	49.5	75.52	-
AFA-FCN	1659.2	51.9	77.88	3.1
U-Net-S5-D16	1622.8	29.1	62.73	-
AFA-U-Net	2146.7	29.4	64.42	2.7
HRNet-W48	748.7	65.9	78.48	-
AFA-HRNet	701.4	65.4	80.41	2.5

AFA-DLA also obtains competitive performance with the top performing method while using around 75% fewer operations and parameters. Compared to other methods, AFA-DLA is more efficient while obtaining better results.

We additionally evaluate the application of AFA to other widely used segmentation models, including FCN, U-Net, and HRNet. Since we only modify the aggregation operations of each model, we can still use the original ImageNet [9] pre-training weights as initialization. A comparison between the original models and their AFA variants in both performance and resource usage is shown in Table 3. Combined with our AFA module, the segmentation models can each obtain at least 2.5% improvement in mIoU, with only a small computational and parameter overhead. In particular, we even lighten HRNet by replacing its concatenation in the last layer with our multiple feature fusion and still achieve 2.5% improvement. This solidifies AFA as a lightweight module that can be readily applied to existing models for segmentation.

4.2 Results on Mapillary Vistas

Mapillary Vistas [23] provides large-scale street-level images. It contains 66 well-annotated object categories for 25K high resolution images with various resolutions ranging from 1024 x 768 to 4000 x 6000. We followed [7, 31] to resize the image such that the longest side is 2176. There are 18K, 2K and 5K images for training, validation and testing, respectively. Due to the enormous amount of training data, we use DLA-169 as the backbone for AFA-DLA. However, we are still limited by computational resources, so the large numbers of categories limits us to only using a crop size of 832 x 832 and a batch size of 16 during training. The results on the Vistas validation set is shown in Table 4.

Despite these limitations, AFA-DLA still achieves competitive results with other methods that use much larger crop sizes. After 200 epochs training, our approach can obtain 57.5 mean IoU on the Vistas validation set.

4.3 Results on BDD100K

BDD100K [40] is a diverse driving video dataset for multi-task learning. For the semantic segmentation task, it provides 10K images with same categories as Cityscapes at 1280 x 720 resolution. The dataset consists 7K, 1K, and 2K images for training, validation, and testing. We also use DLA-169 as the backbone with full image crop and 16 training batch

Table 4: Segmentation results on the Mapillary Vistas validation set. We compare our results with the best performance reported by the other approaches. AFA-DLA achieves competitive results with other methods despite using a much smaller crop size.

Method	Crop Size	mIoU
Seamless [25]	Full Image	50.4
DeeperLab [38]	1441 x 1441	55.3
Axial-DeepLab	2048 x 1024	58.4
Panoptic-DeepLab	1024 x 1024	58.7
HMA [31]	1856 x 1024	61.1
AFA-DLA-169 (Ours)	832 x 832	57.5

Table 5: Segmentation results on BDD100K validation set. † denotes using Cityscapes data for pre-training. AFA-DLA achieves the new state-of-the-art performance.

Method	Backbone	mIoU
DLA-34 [43]	DLA-34	57.84
CCNet [16]	ResNet-101	64.03
Deeplabv3+ [6]	ResNet-101	64.49
DecoupleSegNet† [17]	ResNet-101	66.90
AFA-DLA-169 (Ours)	DLA-169	67.46

size for 200 epochs. To the best of our knowledge, only DecoupleSegNet [17] conducts experiments on the BDD100K validation set, so we compare our results with theirs along with the official provided strong baseline models. The results are shown in Table 5. AFA-DLA achieves the new state-of-the-art performance on the BDD100K validation set.

4.4 Boundary Detection

We additionally conduct experiments on boundary detection, which involves predicting a binary segmentation mask indicating the existence of boundaries. We evaluate on two standard boundary detection datasets, Berkeley Segmentation Data Set and Benchmarks 500 (BSDS500) [1] and NYU Depth Dataset V2 (NYUDv2) [29]. For each dataset, we follow the standard data preprocessing and evaluation protocol in literature [35, 19]. Specifically, we augment each dataset by randomly flipping, scaling, and rotating each image. We evaluate using commonly used metrics, which are the F-measure at the Optimal Dataset Scale (ODS) and at the Optimal Image Scale (OIS). Following [43], we also scale the boundary labels by 10 to account for the label imbalance. For simplicity, we do not consider using multi-scale images during inference, so SSR is not used for these experiments.

Results on BSDS500 The BSDS500 dataset contains 200 training images, 100 validation images, and 200 testing images. We follow standard practice [35] and only use boundaries annotated by three or more annotators for supervision. We do not consider augmenting the training set with additional data, so we only utilize the available data in the BSDS500 dataset.

The results are shown in Table 6. AFA-DLA achieves state-of-the-art performance when comparing to methods

Table 6: Boundary detection results on BSDS500 test set. AFA-DLA outperforms all other methods in ODS.

Method	ODS	OIS
DLA-102 [43]	0.803	0.813
LPCB [10]	0.800	0.816
BDCN [15]	0.806	0.826
AFA-DLA-34 (Ours)	0.812	0.826

Table 7: Boundary detection results on NYUDv2 test set. † indicates only using RGB images as input. AFA-DLA achieves state-of-the-art performance.

Method	ODS	OIS
AFA-DLA-34 (Ours)†	0.762	0.775
AMH-Net [19]	0.771	0.786
BDCN [15]	0.765	0.781
PiDiNet [30]	0.756	0.773
AFA-DLA-34 (Ours)	0.780	0.792

only training on the BSDS500 dataset and obtains a high score of 0.812 in ODS. In particular, AFA-DLA improves the performance of DLA by 0.09 in ODS and 0.013 in OIS, despite using a smaller backbone.

Results on NYUDv2 The NYUDv2 dataset contains both RGB and depth images. There are 381 training images, 414 validation images, and 654 testing images. We follow the same procedure as [35, 19, 15] and train a separate model on RGB and HHA [14] images. We then evaluate using both RGB and HHA images as input by averaging each model’s output during inference.

The results are shown in Table 7. Our AFA-DLA model outperforms all other methods by a large margin, achieving state-of-the-art performance with 0.780 in ODS and 0.792 in OIS. For reference, we also show our model’s performance on only RGB images, which already outperforms some other methods using both RGB and HHA images.

4.5 Ablation Experiments

In this section, we conduct several ablation studies on the Cityscapes validation set to validate each component of AFA-DLA. The main baseline model we compare to is DLA [43] with DLA-34 as backbone. All the results are listed in Table 8. We also provide visualizations in order to qualitatively evaluate our model.

Binary Fusion We first evaluate whether attentive binary fusion provides improvements over standard linear fusion operators. By computing both spatial and channel attention, our attentive binary fusion module can learn and predict the importance of each input signal during fusion. Thus, it not only learns how to distinguish relevant features from redundant ones but also enlarges the receptive field. We observe about 1 mean IoU improvement with our binary fusion module over the original DLA model.

Auxiliary Segmentation Head We add several auxiliary segmentation heads into AFA-DLA to stabilize the training

Table 8: Ablation Study on Cityscapes validation set.

Backbone	Binary Fusion	Aux. Segmentation Head	Multiple Feature Fusion	Multi-scale Inference	mIoU
DLA-34	Original	-	-	Single Scale	74.43
DLA-34	Attentive	-	-	Single Scale	75.56
DLA-34	Attentive	✓	-	Single Scale	76.45
DLA-34	Attentive	✓	✓	Single Scale	77.08
DLA-34	Attentive	✓	✓	Average Pooling	78.56
DLA-34	Attentive	✓	✓	HMA [31]	80.18
DLA-34	Attentive	✓	✓	Scale-Space Rendering Attention	80.74

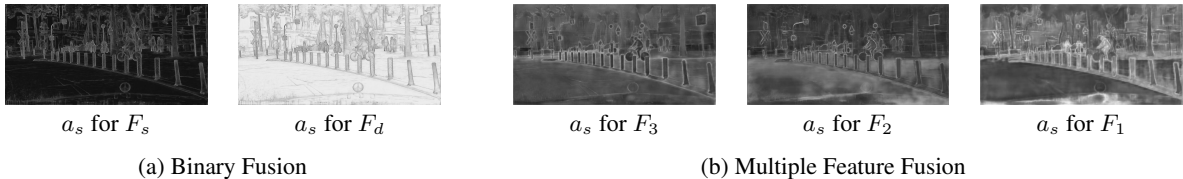
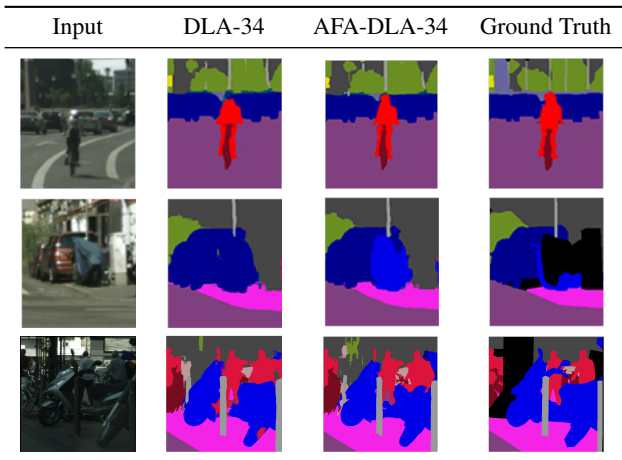
Figure 6: Visualization of spatial attention a_s maps generated by our attentive feature aggregation modules. Whiter regions denote higher attention. Compared to linear fusion operations, our AFA modules provide a more expressive way of combining features.

Figure 7: Comparison of predictions generated by DLA and AFA-DLA. The black pixels are ignored. AFA-DLA can better distinguish object boundaries, such as the human in the first row, and correctly classify object classes, such as the motorcycles in the second and third row.

of attention mechanism, which is common practice among other popular baseline models. The whole backbone can be supervised by the auxiliary losses efficiently and they can alleviate gradient vanishing issues. We see about 1 mean IoU improvement.

Multiple Features Fusion We apply our multiple feature fusion to enable AFA-DLA to fully leverage intermediate features in the network. This gives the network more flexibility in selecting relevant features for computing the final feature. By adding the multiple feature fusion module, we gain another 0.5 mean IoU improvement.

Scale-Space Rendering We employ our SSR module to fuse multi-scale predictions. After applying our SSR with [0.25, 0.5, 1.0, 2.0] inference scales, we gain an impressive improvement of nearly 3.7% mean IoU over using only a single scale. We also compare with different multi-scale inference approaches under the same training setting. SSR gains 1.2 mean IoU over standard average pooling and further outperforms hierarchical multi-scale attention [31] by nearly 0.6 mean IoU. This suggests that our scale-space rendering attention can boost the performance by reducing the gradient vanishing problem and still retain the flexibility for selecting different training and inference scales. With both AFA and SSR, our network improves the DLA baseline model performance by nearly 6.3 mean IoU.

Attention Visualization To understand which parts of the inputs our AFA fusion modules attends to, we visualize the generated attention maps for a set of input features in Figure 6. AFA learns to attend to different regions of the input features depending on the information they contain. For example, our binary fusion module focuses on object boundaries in shallower features and attends to the rest on deeper features. Compared to linear fusion operations, AFA provides a more expressive way of combining features.

Segmentation Visualization We take a deeper look at the segmentation predictions produced by AFA-DLA in Figure 7 and compare them to those produced by DLA [43]. With our AFA module, the model can better leverage spatial and channel information to distinguish object boundaries more clearly and better classify object classes.

5 Conclusion

We proposed a novel attention-based feature aggregation module combined with a new multi-scale inference module to build the competitive AFA-DLA model. With effective spatial and channel self-attention mechanisms, AFA enlarges

the receptive field and enables better propagation of essential information through the network. SSR improves existing multi-scale inference methods by being more robust towards the gradient vanishing problem. Applying all of our components, we improve the DLA baseline model performance by nearly 6.3 mean IoU on Cityscapes. When combining AFA with existing segmentation models, we found consistent improvements of at least 2.5% in mean IoU on Cityscapes, with only a small cost in computational and parameter overhead. AFA-DLA also achieves a new state-of-the-art results on BDD100K, and the new best score on Cityscapes when not using external segmentation datasets. Moreover, for the boundary detection task, AFA-DLA obtains state-of-the-art results on BSDS500 and NYUDv2.

References

- [1] P. Arbeláez, M. Maire, C. Fowlkes, and J. Malik. Contour detection and hierarchical image segmentation. *IEEE Trans. Pattern Anal. Mach. Intell.*, 33(5):898–916, May 2011.
- [2] L. Chen, H. Zhang, J. Xiao, L. Nie, J. Shao, W. Liu, and T.-S. Chua. Sca-cnn: Spatial and channel-wise attention in convolutional networks for image captioning. In *CVPR*, 2017.
- [3] L.-C. Chen, G. Papandreou, I. Kokkinos, K. Murphy, and A. L. Yuille. Deeplab: Semantic image segmentation with deep convolutional nets, atrous convolution, and fully connected crfs. *IEEE transactions on pattern analysis and machine intelligence*, 40(4):834–848, 2017.
- [4] L.-C. Chen, G. Papandreou, F. Schroff, and H. Adam. Rethinking atrous convolution for semantic image segmentation. *arXiv preprint arXiv:1706.05587*, 2017.
- [5] L.-C. Chen, Y. Yang, J. Wang, W. Xu, and A. L. Yuille. Attention to scale: Scale-aware semantic image segmentation. In *Proceedings of the IEEE conference on computer vision and pattern recognition*, pages 3640–3649, 2016.
- [6] L.-C. Chen, Y. Zhu, G. Papandreou, F. Schroff, and H. Adam. Encoder-decoder with atrous separable convolution for semantic image segmentation. In *ECCV*, 2018.
- [7] B. Cheng, M. D. Collins, Y. Zhu, T. Liu, T. S. Huang, H. Adam, and L.-C. Chen. Panoptic-deeplab: A simple, strong, and fast baseline for bottom-up panoptic segmentation. In *CVPR*, 2020.
- [8] M. Cordts, M. Omran, S. Ramos, T. Rehfeld, M. Enzweiler, R. Benenson, U. Franke, S. Roth, and B. Schiele. The cityscapes dataset for semantic urban scene understanding. In *Proc. of the IEEE Conference on Computer Vision and Pattern Recognition (CVPR)*, 2016.
- [9] J. Deng, W. Dong, R. Socher, L.-J. Li, K. Li, and L. Fei-Fei. ImageNet: A Large-Scale Hierarchical Image Database. In *CVPR09*, 2009.
- [10] R. Deng, C. Shen, S. Liu, H. Wang, and X. Liu. Learning to predict crisp boundaries. In *Proceedings of the European Conference on Computer Vision (ECCV)*, pages 562–578, 2018.
- [11] R. A. Drebin, L. Carpenter, and P. Hanrahan. Volume rendering. In *Proceedings of the 15th Annual Conference on Computer Graphics and Interactive Techniques, SIGGRAPH '88*, page 65–74, New York, NY, USA, 1988. Association for Computing Machinery.
- [12] J. Fu, J. Liu, H. Tian, Y. Li, Y. Bao, Z. Fang, and H. Lu. Dual attention network for scene segmentation. In *Proceedings of the IEEE Conference on Computer Vision and Pattern Recognition*, pages 3146–3154, 2019.
- [13] J. Fu, J. Liu, Y. Wang, Y. Li, Y. Bao, J. Tang, and H. Lu. Adaptive context network for scene parsing. In *Proceedings of the IEEE/CVF International Conference on Computer Vision*, pages 6748–6757, 2019.
- [14] S. Gupta, R. Girshick, P. Arbeláez, and J. Malik. Learning rich features from rgb-d images for object detection and segmentation. In *European conference on computer vision*, pages 345–360. Springer, 2014.
- [15] J. He, S. Zhang, M. Yang, Y. Shan, and T. Huang. Bi-directional cascade network for perceptual edge detection. In *Proc. of the IEEE Conference on Computer Vision and Pattern Recognition (CVPR)*, 2019.
- [16] Z. Huang, X. Wang, Y. Wei, L. Huang, H. Shi, W. Liu, and T. S. Huang. Ccnet: Criss-cross attention for semantic segmentation. *IEEE Transactions on Pattern Analysis and Machine Intelligence*, pages 1–1, 2020.
- [17] X. Li, X. Li, L. Zhang, C. Guangliang, J. Shi, Z. Lin, Y. Tong, and S. Tan. Improving semantic segmentation via decoupled body and edge supervision. In *ECCV*, 2020.
- [18] D. Lin, D. Shen, S. Shen, Y. Ji, D. Lischinski, D. Cohen-Or, and H. Huang. Zigzagnet: Fusing top-down and bottom-up context for object segmentation. In *2019 IEEE/CVF Conference on Computer Vision and Pattern Recognition (CVPR)*, pages 7482–7491, 2019.
- [19] Y. Liu, M.-M. Cheng, X. Hu, K. Wang, and X. Bai. Richer convolutional features for edge detection. In *Proc. of the IEEE Conference on Computer Vision and Pattern Recognition (CVPR)*, 2017.
- [20] J. Long, E. Shelhamer, and T. Darrell. Fully convolutional networks for semantic segmentation. In *Proceedings of the IEEE conference on computer vision and pattern recognition*, pages 3431–3440, 2015.
- [21] B. Mildenhall, P. P. Srinivasan, M. Tancik, J. T. Barron, R. Ramamoorthi, and R. Ng. Nerf: Representing scenes as neural radiance fields for view synthesis. In *European Conference on Computer Vision*, pages 405–421. Springer, 2020.
- [22] R. Mottaghi, X. Chen, X. Liu, N.-G. Cho, S.-W. Lee, S. Fidler, R. Urtasun, and A. Yuille. The role of context for object detection and semantic segmentation in the wild. In *2014 IEEE Conference on Computer Vision and Pattern Recognition*, pages 891–898, 2014.

- [23] G. Neuhold, T. Ollmann, S. Rota Bulò, and P. Kotschieder. The mapillary vistas dataset for semantic understanding of street scenes. In *International Conference on Computer Vision (ICCV)*, 2017.
- [24] A. Paszke, S. Gross, F. Massa, A. Lerer, J. Bradbury, G. Chanan, T. Killeen, Z. Lin, N. Gimelshein, L. Antiga, A. Desmaison, A. Kopf, E. Yang, Z. DeVito, M. Raison, A. Tejani, S. Chilamkurthy, B. Steiner, L. Fang, J. Bai, and S. Chintala. Pytorch: An imperative style, high-performance deep learning library. In H. Wallach, H. Larochelle, A. Beygelzimer, F. d'Alché-Buc, E. Fox, and R. Garnett, editors, *Advances in Neural Information Processing Systems 32*, pages 8024–8035. Curran Associates, Inc., 2019.
- [25] L. Porzi, S. Rota Bulò, A. Colovic, and P. Kotschieder. Seamless scene segmentation. In *The IEEE Conference on Computer Vision and Pattern Recognition (CVPR)*, June 2019.
- [26] H. Robbins and S. Monro. A Stochastic Approximation Method. *The Annals of Mathematical Statistics*, 22(3):400 – 407, 1951.
- [27] O. Ronneberger, P. Fischer, and T. Brox. U-net: Convolutional networks for biomedical image segmentation. In *International Conference on Medical image computing and computer-assisted intervention*, pages 234–241. Springer, 2015.
- [28] S. Rota Bulò, L. Porzi, and P. Kotschieder. In-place activated batchnorm for memory-optimized training of dnns. In *Proceedings of the IEEE Conference on Computer Vision and Pattern Recognition*, 2018.
- [29] N. Silberman, D. Hoiem, P. Kohli, and R. Fergus. Indoor segmentation and support inference from rgb-d images. In *Computer Vision, ECCV 2012 - 12th European Conference on Computer Vision, Proceedings*, 2012.
- [30] Z. Su, W. Liu, Z. Yu, D. Hu, Q. Liao, Q. Tian, M. Pietikäinen, and L. Liu. Pixel difference networks for efficient edge detection. *arXiv preprint arXiv:2108.07009*, 2021.
- [31] A. Tao, K. Sapra, and B. Catanzaro. Hierarchical multi-scale attention for semantic segmentation. *arXiv preprint arXiv:2005.10821*, 2020.
- [32] H. Wang, Y. Zhu, B. Green, H. Adam, A. Yuille, and L.-C. Chen. Axial-deeplab: Stand-alone axial-attention for panoptic segmentation. In *European Conference on Computer Vision (ECCV)*, 2020.
- [33] J. Wang, K. Sun, T. Cheng, B. Jiang, C. Deng, Y. Zhao, D. Liu, Y. Mu, M. Tan, X. Wang, et al. Deep high-resolution representation learning for visual recognition. *IEEE transactions on pattern analysis and machine intelligence*, 2020.
- [34] S. Woo, J. Park, J.-Y. Lee, and I. S. Kweon. Cbam: Convolutional block attention module. In *Proceedings of the European conference on computer vision (ECCV)*, pages 3–19, 2018.
- [35] S. Xie and Z. Tu. Holistically-nested edge detection. In *2015 IEEE International Conference on Computer Vision (ICCV)*, pages 1395–1403, 2015.
- [36] M. Yang, K. Yu, C. Zhang, Z. Li, and K. Yang. Denseaspp for semantic segmentation in street scenes. In *2018 IEEE/CVF Conference on Computer Vision and Pattern Recognition*, pages 3684–3692, 2018.
- [37] S. Yang and G. Peng. Attention to refine through multi scales for semantic segmentation. In *Pacific Rim Conference on Multimedia*, pages 232–241. Springer, 2018.
- [38] T.-J. Yang, M. D. Collins, Y. Zhu, J.-J. Hwang, T. Liu, X. Zhang, V. Sze, G. Papandreou, and L.-C. Chen. Deeplab: Single-shot image parser. *arXiv preprint arXiv:1902.05093*, 2019.
- [39] M. Yin, Z. Yao, Y. Cao, X. Li, Z. Zhang, S. Lin, and H. Hu. Disentangled non-local neural networks. *arXiv preprint arXiv:2006.06668*, 2020.
- [40] F. Yu, H. Chen, X. Wang, W. Xian, Y. Chen, F. Liu, V. Madhavan, and T. Darrell. Bdd100k: A diverse driving dataset for heterogeneous multitask learning. In *Proceedings of the IEEE/CVF Conference on Computer Vision and Pattern Recognition (CVPR)*, June 2020.
- [41] F. Yu and V. Koltun. Multi-scale context aggregation by dilated convolutions. *arXiv preprint arXiv:1511.07122*, 2015.
- [42] F. Yu, V. Koltun, and T. Funkhouser. Dilated residual networks. In *Computer Vision and Pattern Recognition (CVPR)*, 2017.
- [43] F. Yu, D. Wang, E. Shelhamer, and T. Darrell. Deep layer aggregation. In *2018 IEEE/CVF Conference on Computer Vision and Pattern Recognition*, pages 2403–2412, 2018.
- [44] Y. Yuan, X. Chen, and J. Wang. Object-contextual representations for semantic segmentation. *arXiv preprint arXiv:1909.11065*, 2020.
- [45] Y. Yuan, J. Xie, X. Chen, and J. Wang. Segfix: Model-agnostic boundary refinement for segmentation. *arXiv preprint arXiv:2007.04269*, 2020.
- [46] Y. Yuan, J. Xie, X. Chen, and J. Wang. Segfix: Model-agnostic boundary refinement for segmentation. *arXiv preprint arXiv:2007.04269*, 2020.
- [47] H. Zhao, X. Qi, X. Shen, J. Shi, and J. Jia. Icnets for real-time semantic segmentation on high-resolution images. In *Proceedings of the European conference on computer vision (ECCV)*, pages 405–420, 2018.
- [48] H. Zhao, J. Shi, X. Qi, X. Wang, and J. Jia. Pyramid scene parsing network. In *CVPR*, 2017.
- [49] S. Zhao, Y. Wang, Z. Yang, and D. Cai. Region mutual information loss for semantic segmentation. *arXiv preprint arXiv:1910.12037*, 2019.
- [50] Y. Zhu, K. Sapra, F. A. Reda, K. J. Shih, S. Newsam, A. Tao, and B. Catanzaro. Improving semantic segmentation via video propagation and label relaxation. In *Proceedings of the IEEE/CVF Conference on Computer Vision and Pattern Recognition*, pages 8856–8865, 2019.

A Appendix

In this appendix, we provide additional results on boundary detection benchmarks, detailed explanations about the vanishing gradients issue and training settings, and visualizations of attention maps and output predictions.

A.1 Full Results on Boundary Detection Benchmarks

To complete the results in Table 6 and Table 7 in the main paper, we provide the full evaluation results on BSDS500 [1] in Table 10 and on NYUDv2 [29] in Table 11.

On BSDS500, we show more evaluation results of using the PASCAL VOC Context dataset (PVC) [22] as additional training data and multi-scale inference. When using PVC, we double our training epochs to account for the additional data. For multi-scale inference, we use standard average pooling for fair comparison with other methods. AFA-DLA achieves state-of-the-art results on single-scale inference when not training with additional data. Surprisingly, using PVC does not further improve the results. Nevertheless, AFA-DLA achieves the same performance with the state-of-the-art method BDCN [15] when using multi-scale inference.

On NYUDv2, we further show evaluation results of using a single image as input for both RGB and HHA images. AFA-DLA outperforms other methods across both settings. In particular, on RGB images, AFA-DLA can obtain 0.014 improvement in ODS and 0.012 improvement in OIS over the best performing competitor. When combining RGB and HHA images, AFA-DLA achieves state-of-the-art results.

A.2 Results on BDD100K Testing Benchmark

We submit our testing set results after the BDD100K [40] releases its official benchmark. As shown in Table 9, Our AFA-DLA achieves new state-of-the-art performance among of the official provided strong baseline models.

A.3 Vanishing Gradients with Attention Mechanisms

We go into more depth regarding the vanishing gradient issues with existing attention mechanisms. To see this, consider the Jacobian of the attention coefficients, which takes the following form:

$$J_{i\ell} \triangleq \frac{\partial \alpha_i(y)}{\partial y_\ell} = \begin{cases} \phi'(y_i) \prod_{j=1}^i e^{-\phi(y_j)} & \text{if } \ell = i \\ 0 & \text{if } \ell > i \\ -\phi'(y_\ell) \alpha_i(y) & \text{if } \ell < i. \end{cases}$$

In the presence of two scales, this becomes:

$$J = \begin{bmatrix} \phi'(y_1) a_1 & 0 \\ -\phi'(y_1) a_1 (1 - a_2) & \phi'(y_2) a_1 a_2, \end{bmatrix}$$

where $a_i \triangleq e^{-\phi(y_i)}$. As $a_1 \rightarrow 0$, the gradient vanishes, for J tends to a null matrix. Otherwise, irrespective of the value of a_2 , the gradient will vanish only depending on the choice of ϕ . In particular, by taking the absolute value as ϕ we have that the Jacobian will not vanish for $a_1 > 0$ and $(y_1, y_2) \neq (0, 0)$, thus motivating our choice of using the absolute value as ϕ . If

Table 9: Segmentation results on BDD100K testing Benchmark. AFA-DLA achieves the new state-of-the-art performance.

Method	Backbone	mIoU
DNL [39]	ResNet-101	56.31
PSPNet [48]	ResNet-101	56.32
Deeplabv3+ [6]	ResNet-101	57.00
AFA-DLA-169 (Ours)	DLA-169	58.47

Table 10: Boundary detection results on BSDS500 test set. PVC indicates training with the additional PASCAL VOC Context dataset. MS indicates using multi-scale inference. AFA-DLA achieves state-of-the-art results on single-scale images without using additional data, and competitive results when using both PVC and MS.

Method	PVC	MS	ODS	OIS
Human			0.803	0.803
DLA-102 [43]			0.803	0.813
LPCB [10]			0.800	0.816
BDCN [15]			0.806	0.826
AFA-DLA-34 (Ours)			0.812	0.826
RCF [19]	✓		0.808	0.825
LPCB [10]	✓		0.808	0.824
BDCN [15]	✓		0.820	0.838
PiDiNet [30]	✓		0.807	0.823
AFA-DLA-34 (Ours)	✓		0.810	0.826
RCF [19]	✓	✓	0.814	0.833
LPCB [10]	✓	✓	0.815	0.834
BDCN [15]	✓	✓	0.828	0.844
AFA-DLA-34 (Ours)	✓	✓	0.828	0.844

we consider instead the setting in [31], we have that $a_2 = 0$ and $\phi'(y_i) = 1 - a_i$. It follows that the Jacobian vanishes also as $a_1 \rightarrow 1$. The conclusion is that the choice of ϕ plays a role in determining the amount of gradient that flows through the predicted attention and that the approach in HMA [31] is more subject to vanishing gradient issues than our proposed solution.

A.4 Training Losses

In this section, we describe in more detail the formulation of our loss function for AFA-DLA for both semantic segmentation and boundary detection.

Semantic Segmentation We use k scales for training and RMI [49] to be the primary loss for our final prediction P_{final} , i.e.,

$$L_{\text{primary}} \triangleq L_{\text{rmi}}(\hat{P}, P_{\text{final}}),$$

where \hat{P} is the ground truth and L_{rmi} is the RMI loss function. The first auxiliary cross-entropy loss is computed by using the generated scale-space rendering (SSR) attention to fuse the auxiliary per-scale predictions from the OCR [44] module, yielding

$$L_{\text{ocr}} \triangleq L_{\text{ce}}(\hat{P}, P_{\text{ocr}}^{\text{aux}}),$$

where L_{ce} denotes the cross-entropy loss. For the second auxiliary loss, we compute and sum up cross-entropy losses

Table 11: Boundary detection results on NYUDv2 test set using three different types of inputs. AFA-DLA achieves state-of-the-art results across all three settings.

Method	Input	ODS	OIS
AMH-Net [19]	RGB	0.744	0.758
BDCN [15]	RGB	0.748	0.763
PiDiNet [30]	RGB	0.733	0.747
AFA-DLA-34 (Ours)	RGB	0.762	0.775
AMH-Net [19]	HHA	0.716	0.729
BDCN [15]	HHA	0.707	0.719
PiDiNet [30]	HHA	0.715	0.728
AFA-DLA-34 (Ours)	HHA	0.718	0.730
AMH-Net [19]	RGB+HHA	0.771	0.786
BDCN [15]	RGB+HHA	0.765	0.781
PiDiNet [30]	RGB+HHA	0.756	0.773
AFA-DLA-34 (Ours)	RGB+HHA	0.780	0.792

for each scale prediction P_i , where $1 \leq i \leq k$, yielding

$$L_{\text{scale}} \triangleq \sum_{i=1}^k L_{\text{ce}}(\hat{P}, P_i).$$

Lastly, for the auxiliary loss inside AFA-DLA, we fuse the predictions of each auxiliary segmentation head with SSR across scales and get P_j^{aux} , where $1 \leq j \leq 4$. We compute the auxiliary loss for each prediction and sum them up as

$$L_{\text{dla}} \triangleq \sum_{j=1}^4 L_{\text{ce}}(\hat{P}, P_j^{\text{aux}}).$$

Accordingly, the total loss function is the weighted sum as

$$L_{\text{seg}} \triangleq L_{\text{primary}} + \beta_o L_{\text{ocr}} + \beta_s L_{\text{scale}} + \beta_d L_{\text{dla}},$$

where we set $\beta_o = 0.4$, $\beta_s = 0.05$, and $\beta_d = 0.05$.

Boundary Detection For boundary detection, we opted to using a simpler version of the loss function for semantic segmentation. We use standard binary cross entropy (BCE) to be the primary loss for our final prediction P_{final} , i.e.,

$$L_{\text{primary}} \triangleq L_{\text{bce}}(\hat{P}, P_{\text{final}}),$$

where \hat{P} is the ground truth and L_{bce} is the BCE loss function.

We also use auxiliary segmentation heads to make predictions at each feature level. Each prediction P_j^{aux} , where $1 \leq j \leq 4$, is upsampled to the original scale and the BCE loss is used to compute the auxiliary loss, i.e.,

$$L_{\text{dla}} \triangleq \sum_{j=1}^4 L_{\text{bce}}(\hat{P}, P_j^{\text{aux}}).$$

Accordingly, the total loss function is the weighted sum as

$$L_{\text{bd}} \triangleq L_{\text{primary}} + \beta_d L_{\text{dla}},$$

where we set $\beta_d = 0.05$.

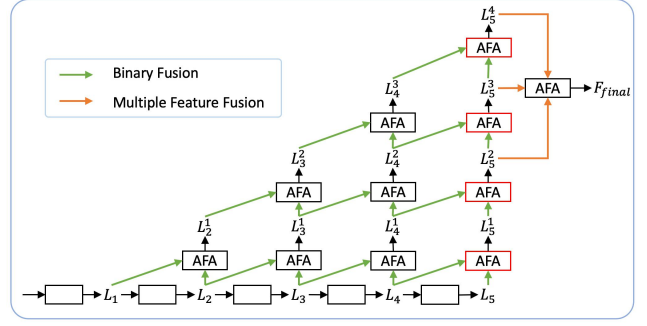


Figure 8: Notation of aggregated features of AFA-DLA.

Table 12: Specific training settings for each dataset.

Dataset	Crop Size	Batch Size	Total Epochs
Cityscapes	2048 x 1024	8	375
Mapillary Vistas	832 x 832	16	200
BDD100K	1280 x 720	16	200
BSDS500	416 x 416	16	10
NYUDv2	480 x 480	16	54

A.5 Implementation Details

We provide the general training setting and procedure used for training on Cityscapes [8], Mapillary Vistas [23], BDD100K [40], BSDS500 [1], and NYUDv2 [29].

We use PyTorch [24] as our framework and develop based on the NVIDIA semantic segmentation codebase¹. The general training procedure is using SGD [26] with momentum of 0.9 and weight decay of 10^{-4} . Specific settings for each dataset are shown in Table 12.

Semantic Segmentation We use an initial learning rate of 1.0×10^{-2} . We use the learning rate warm-up over the initial 1K training iterations and the polynomial decay schedule, which decays the initial learning rate by multiplying $(1 - \frac{\text{epoch}}{\text{max_epochs}})^{0.9}$ every epoch. We apply random image horizontal flipping, randomly rotating within 10 degrees, random scales from 0.5 to 2.0, random image color augmentation, and random cropping. As in [50], we also use class uniform sampling in the data loader to overcome the data class distribution unbalance problem. Due to limitations in computational power, we further use Inplace-ABN [28] to replace the batch norm and ReLU function to acquire the largest possible training crop size and batch size on 8 Tesla V-100 32G GPUs.

Boundary Detection We use an initial learning rate of 1.0×10^{-2} and a batch size of 16 for both BSDS500 [1] and NYUDv2 [29]. We use the step decay schedule and drop the learning rate by 10 times at around $0.55 \times \text{max_epochs}$ and then again at $0.85 \times \text{max_epochs}$. For augmentation, we follow the standard protocol in literature [35, 19] and apply random flipping, scaling by 0.5 and 1.5, and rotation by 16 different angles. We train all our models on a single GeForce RTX 2080Ti GPU.

¹NVIDIA license: <https://github.com/NVIDIA/semantic-segmentation/blob/main/LICENSE>

A.6 Visualization of Attention Maps

In this section, we provide more visualizations of attention maps generated by our proposed AFA module. For reference, we provide a detailed architecture of AFA-DLA and denote the notation of aggregated features of different levels in Figure 8.

We first look at the attention maps generated by our binary fusion module which aggregates two features in Figure 9 and Figure 10. We provide the spatial attention maps for binary fusion at four different levels. When the difference of the level information between two input features is larger (e.g., L_4^3 and L_5^3), our attention mask will become more specific and be able to focus on the right place to be fused. Take the fusion of L_4^3 and L_5^3 as example. Since L_4^3 contains the information of the L_1 feature, our attention focuses on object boundaries on it and attend to the rest on L_5^3 , which has richer semantic information. Compared to linear fusion operations, our AFA module provides a more expressive way of combining features.

We additionally look at the spatial attention maps generated by our multiple feature fusion module in Figure 11. Only using the final aggregated features for prediction may cause our model to overly focus on low level features. Thus, our multiple feature fusion module provides the model with more flexibility to select between the features that contain different low level information. For input features that contain L_1 information like L_5^4 and L_5^3 , the attention focuses more on the object boundaries, similar to our binary fusion module. For other input features like L_5^2 , the attention can focus on objects or the background. With our multiple feature fusion module, our model can strike a balance between the low-level and the high-level information and perform fusion accordingly.

A.7 Qualitative Results

We provide more qualitative results in this section to visualize AFA-DLA’s predictions.

We show full predictions of AFA-DLA on Cityscapes in Figure 12, Mapillary Vistas in Figure 13, BDD100K in Figure 14, BSDS500 in Figure 15, and NYUDv2 in Figure 16. The results on Cityscapes show that our model can handle both fine and coarse details well and is robust towards different input scenes. On Mapillary Vistas, our model can deal with the large amounts of object classes with varying input image sizes and much greater variety of scenes. On BDD100K, the results show the ability of our model to handle more diverse urban scenes, with varying weather conditions and times of the day. On both BSDS500 and NYUDv2, our model can predict both fine-grained scene details as well as object-level boundaries. In particular, on NYUDv2, our model can recover more boundaries than the ground truth. With results across different types of datasets and both semantic segmentation and boundary detection, AFA-DLA demonstrates its strong performance and applicability for dense prediction tasks.

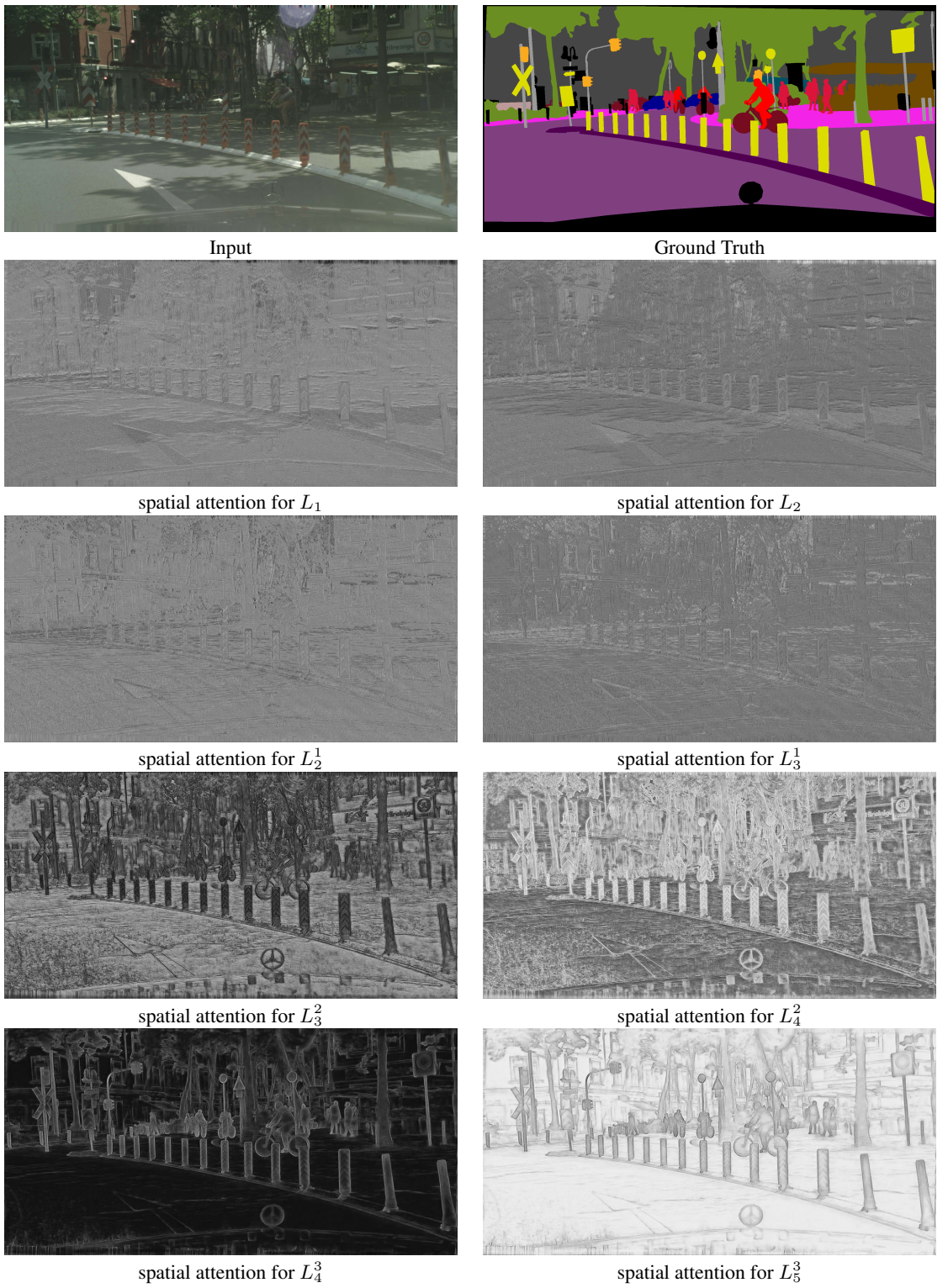


Figure 9: Spatial attention maps at four different levels generated by our binary fusion module which aggregates two features. Whiter regions denote higher attention. Compared to linear fusion operations, our AFA module provides a more expressive way of combining features.

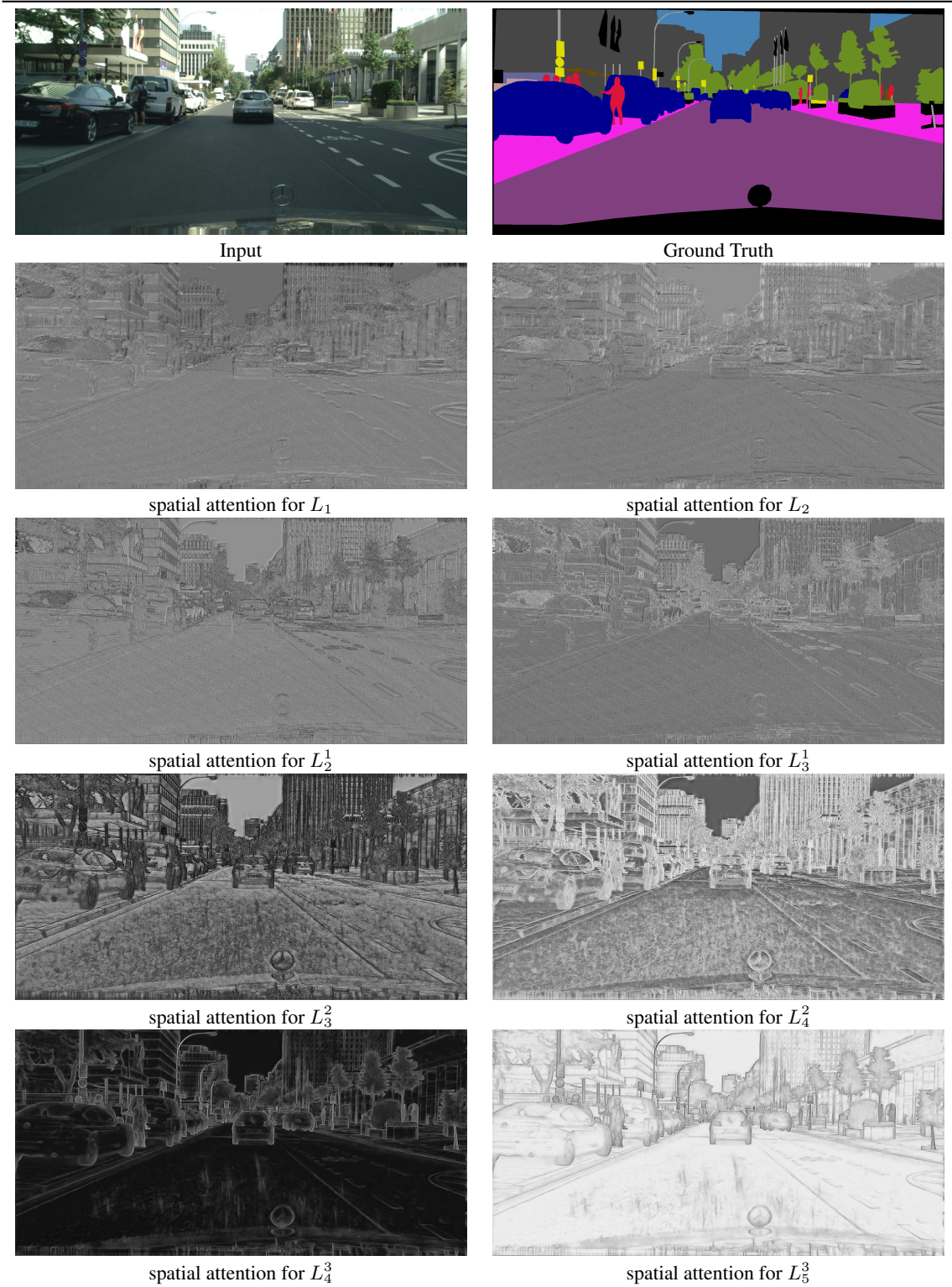


Figure 10: Spatial attention maps at four different levels generated by our binary fusion module which aggregates two features. Whiter regions denote higher attention. Compared to linear fusion operations, our AFA module provides a more expressive way of combining features.

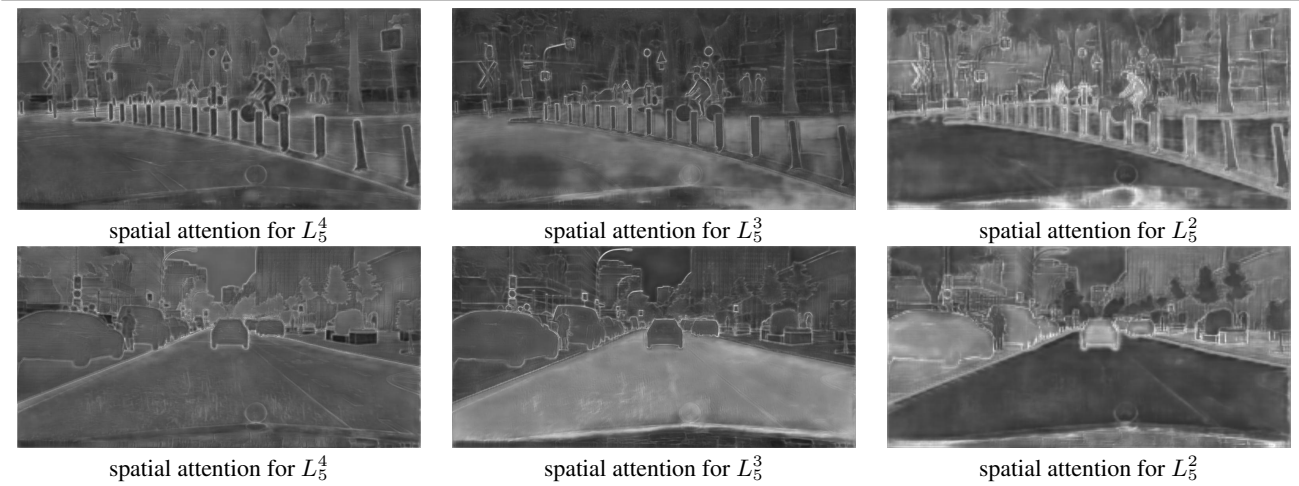


Figure 11: Spatial attention maps generated by our multiple feature fusion module which aggregates multiple features. Whiter regions denote higher attention. With our multiple feature fusion module, our model can strike a balance between the low-level and the high-level information and perform fusion accordingly.

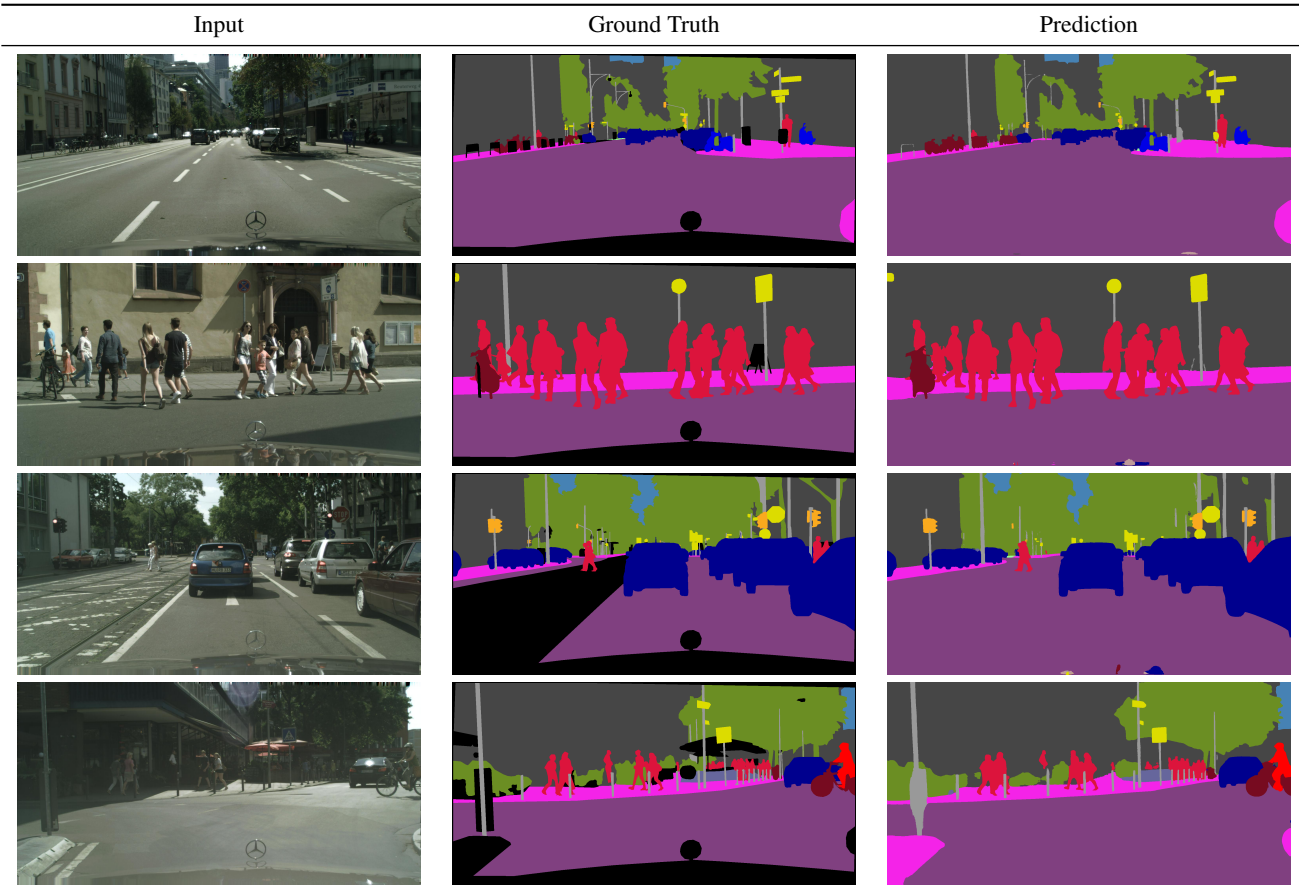


Figure 12: The qualitative results of AFA-DLA-X-102 on the Cityscapes validation set. Our model can handle both fine and coarse details well and is robust towards different input scenes.

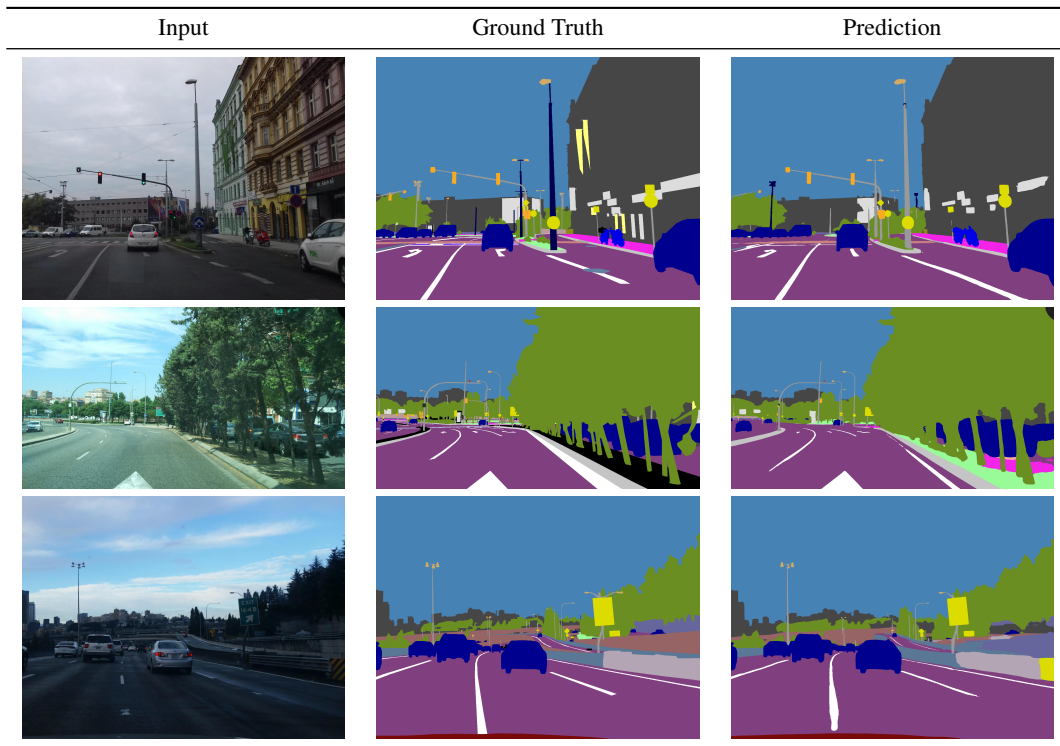


Figure 13: The qualitative results of AFA-DLA-169 on the Mapillary Vistas validation set. Our model can deal with the large amounts of object classes with varying input image sizes and large variety of scenes.

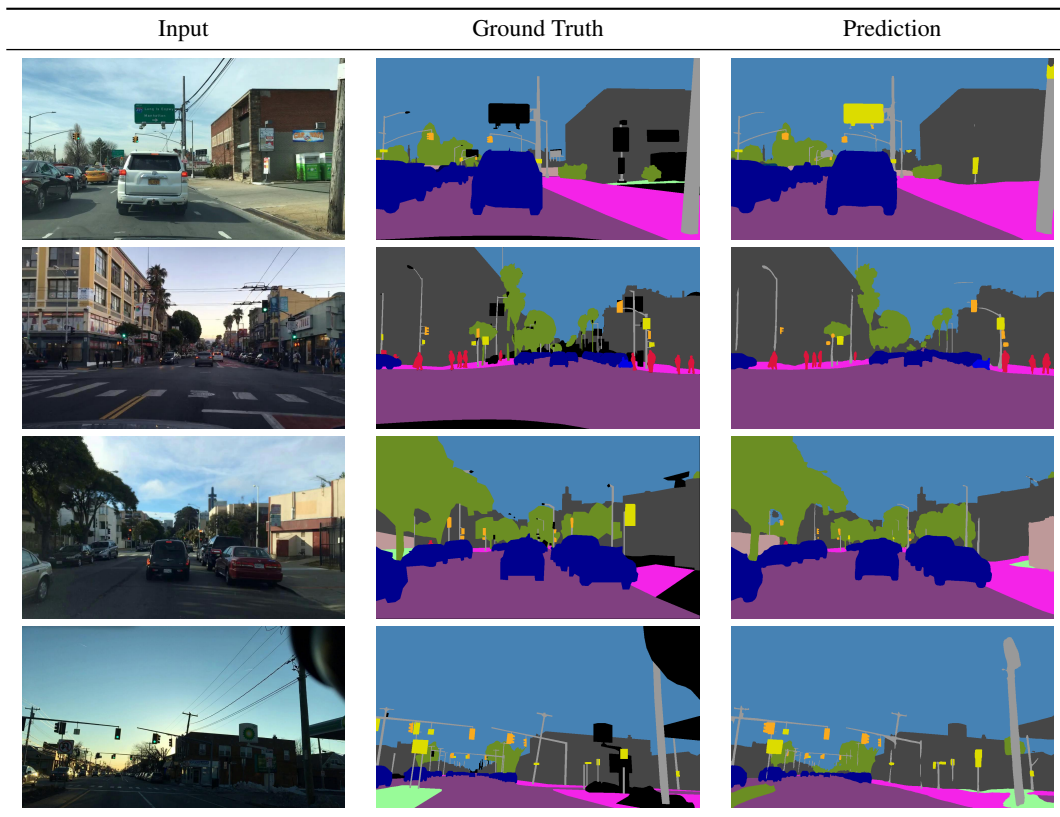


Figure 14: The qualitative results of AFA-DLA-169 on the BDD100K validation set. Our model can handle diverse urban scenes, with varying weather conditions and times of the day.

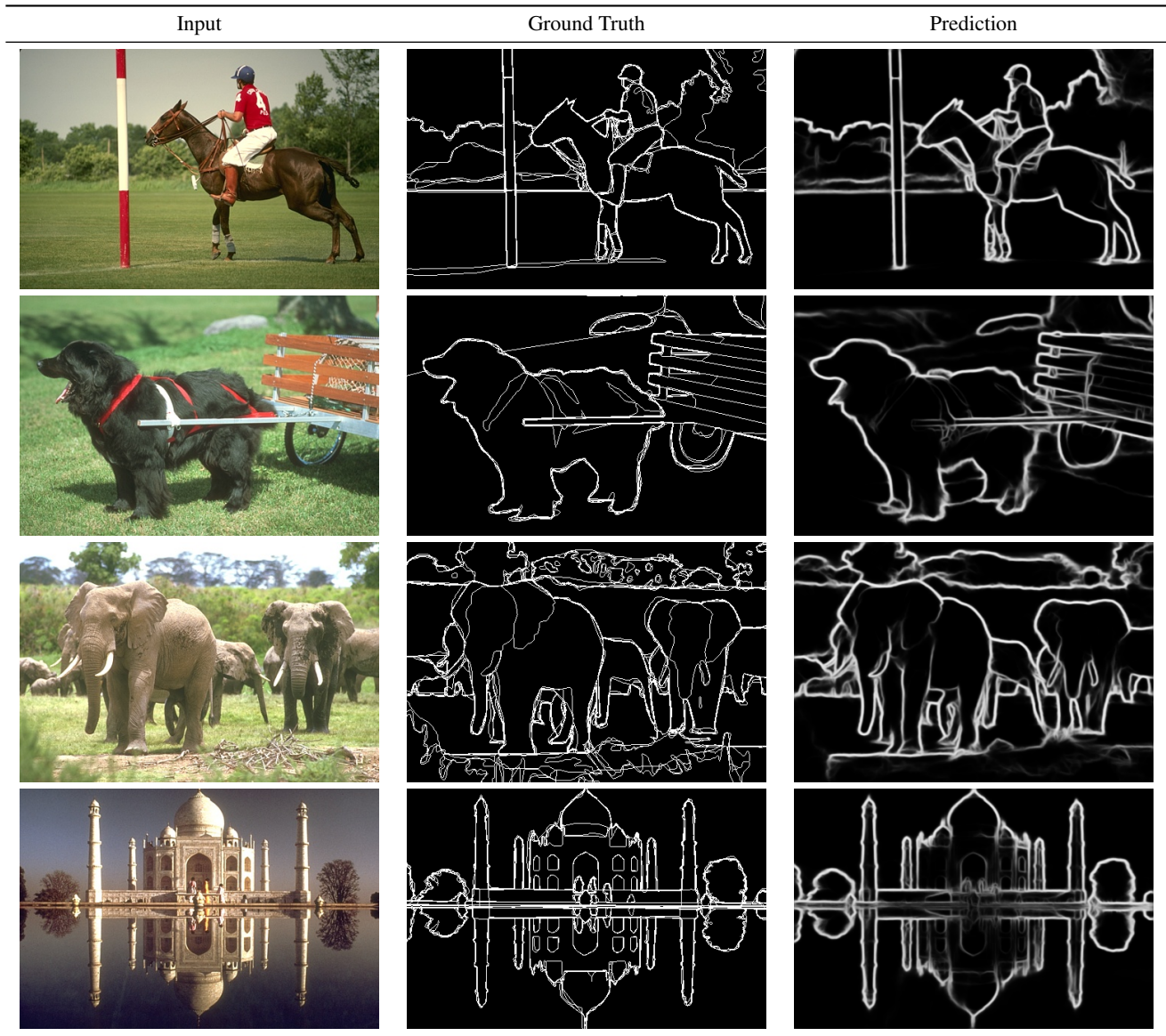


Figure 15: Qualitative results of AFA-DLA-34 on the BSDS500 test set. Results are raw boundary maps obtained using multi-scale inference before Non-Maximum Suppression. Our model can predict both fine-grained scene details as well as object-level boundaries.

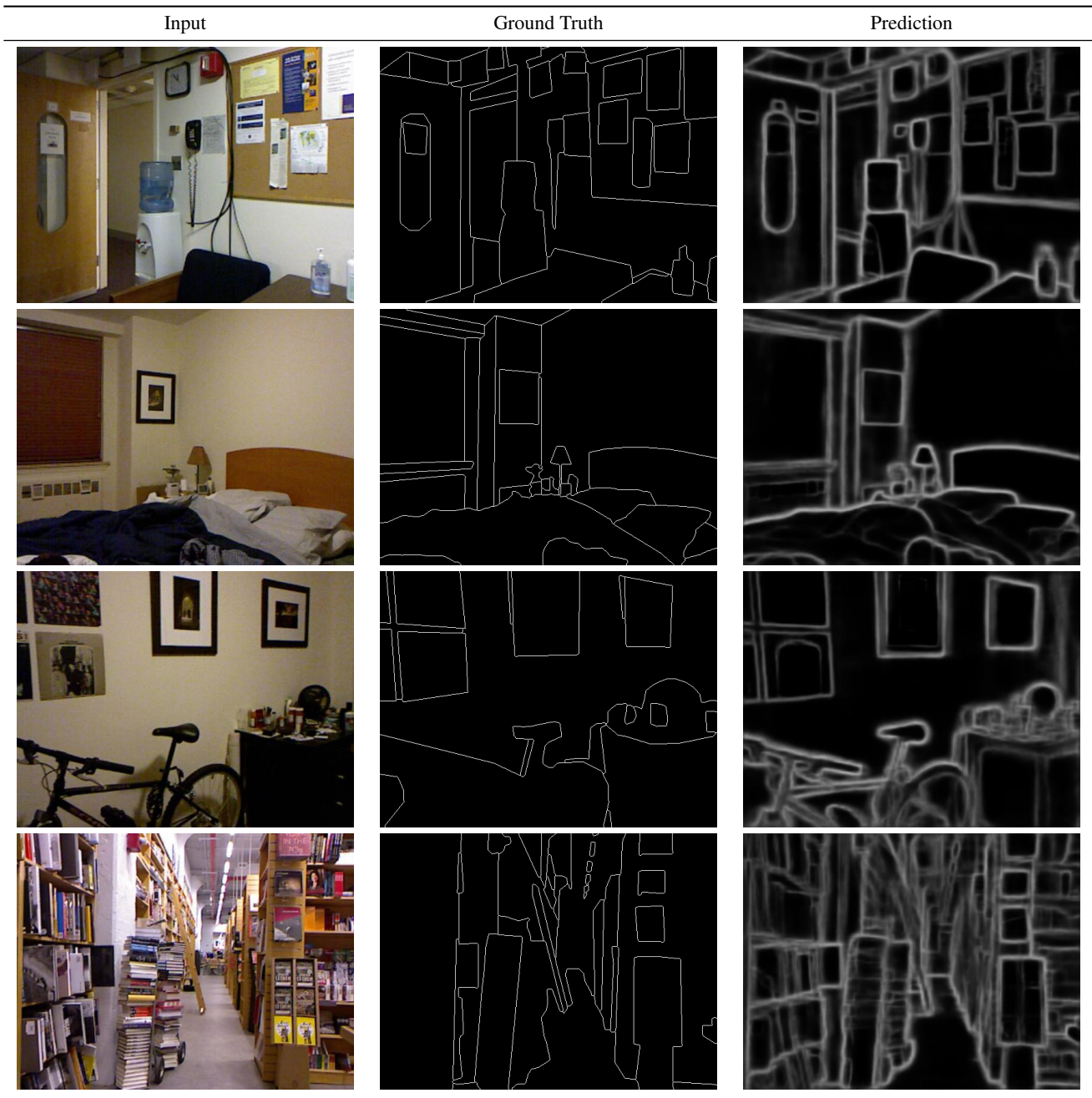


Figure 16: Qualitative results of AFA-DLA-34 on the NYUDv2 test set. Results are raw boundary maps obtained by averaging predictions on both RGB and HHA images before Non-Maximum Suppression. Our model can extract more boundaries than the ground truth.